Supporting Information

Ultrastable Polymolybdate-Based Metal-Organic Frameworks as Highly Active Electrocatalysts for Hydrogen Generation from Water

Jun-Sheng Qin,[†,§] Dong-Ying Du,[†] Wei Guan,[†] Xiang-Jie Bo,[†] Ya-Fei Li,[‡] Li-Ping Guo,[†] Zhong-Min Su,[*,†] Yuan-Yuan Wang,[†] Ya-Qian Lan,[*,†,‡] and Hong-Cai Zhou[*,§]

[†] Institute of Functional Material Chemistry, Key Lab of Polyoxometalate Science of Ministry of Education, Department of Chemistry, Northeast Normal University, Changchun 130024, P. R. China

[‡] School of Chemistry and Materials Science, Nanjing Normal University, Nanjing 210046, P. R. China

[§] Department of Chemistry, Texas A&M University, College Station, TX 77843-3255, USA

S1. Computational details

S1.1 The binding energy (ΔE_b)

As shown in Figure S2, two simplified model structures **1** and **2** were extracted form crystal structures. All single-point calculations were performed using the B3PW91 functional.[1] The LANL2DZ basis set was employed for the Zn and Mo with Los Alamos relativistic effective core potentials (ECPs),[2] while the 6-31G* basis set was used for the other main-group elements. The solvent effect of water was evaluated by the conductor-like polarizable continuum model (CPCM).[3] The binding energy (ΔE_b) between two fragments was evaluated by the equation, $\Delta E_b = E_{(complex)} - E_{(fragment\ A)} - E_{(fragment\ B)}$, based on the ground state. All these calculations were carried out with the Gaussian 09 program.[4]

S1.2 The Gibbs free energy (ΔG)

The spin-polarized DFT computations employed an all-electron method within a generalized gradient approximation (GGA) for the exchange-correlation term, as implemented in the DMol^3 code.[5] The double numerical plus polarization (DNP) basis set and PBE functional[6] were adopted. Self-consistent field (SCF) calculations were performed with a convergence criterion of 10^{-6} a.u. on the total energy and electronic computations.

The change in Gibbs free energy (ΔG) was evaluated for hydrogen adsorption on Zn-ε-Keggin-Cl, as defined as

$$\Delta G = \Delta E + \Delta E_{zpe} - T\Delta S + \Delta G_{pH}$$

The adsorption energy (ΔE) can be directly determined by analyzing the DFT total energies. ΔE_{ZPE} and ΔS are the zero point energy difference and the entropy difference between the adsorbed state and the gas phase, respectively, and T is the system temperature (298.15 K, in this work). For each system, its E_{zpe} can be calculated by summing vibrational frequencies over all normal modes ν ($E_{zpe} = 1/2\Sigma\hbar\nu$). Especially, the free energy of proton and electron ($H^+ + e^-$) at standard conditions was taken as $1/2G_{H2}$.

S2. The preparation of $\varepsilon(trim)_{4/3}$, NENU-5, and HKUST-1

$\varepsilon(trim)_{4/3}$, NENU-5, and HKUST-1 were synthesized according to the procedures described in the literatures[7-9] with little modification.

S2.1 Preparation of $\varepsilon(trim)_{4/3}$[7]

A mixture of $(NH_4)_6Mo_7O_{24}\cdot 4H_2O$ (0.618 g, 0.50 mmol), molybdenum powder 99.99% (0.060 g, 0.62 mmol), H_3PO_3 (0.020 g, 0.25 mmol), $ZnCl_2$ (0.136 g, 1.00 mmol), 1,3,5-benzenetricarboxylic acid (H_3BTC, 0.21 g, 1.00 mmol), tetrabutylammonium hydroxide 40 wt % solution in water (160 μL, 0.24 mmol), and H_2O (8 mL) was stirred, and the pH was adjusted to 5 with 2 M HCl. Then, the mixture was transferred and sealed in a 15 mL Teflonlined stainless steel container, and heated at 180 °C for 72 h. After cooling to room temperature at 10 $°C\cdot h^{-1}$, dark red cubic crystals suitable for X-ray diffraction study were collected after filtration.

S2.2 Preparation of NENU-5[8]

A mixture of $Cu(NO_3)_2\cdot 3H_2O$ (0.24 g, 1.00 mmol) and $H_3PMo_{12}O_{40}\cdot nH_2O$ (0.2 g) in distilled water (10 mL) was stirred for 15 min, and then H_3BTC (0.21 g, 1.00 mmol) and $(CH_3)_4NOH$ (0.09 g, 1.00 mmol) were added in succession with stirring for another 30 min at room temperature. The turbid mixture (pH = 2 − 3) was sealed in a Teflonlined stainless steel container and heated at 180 °C for 24 h, followed by cooling to room temperature at 10 $°C\cdot h^{-1}$, blue octahedral crystals were then harvested.

S2.3 Preparation of HKUST-1[9]

A mixture of $Cu(NO_3)_2\cdot 3H_2O$ (0.24 g, 1.00 mmol) and H_3BTC (0.21 g, 1.00 mmol) in mixed solvent (H_2O:EtOH, 5 mL:5 mL) was stirred for 15 min. The mixture was then sealed in a Teflonlined stainless steel container and heated at 180 °C for 24 h, followed by cooling to room temperature at 10 $°C\cdot h^{-1}$, blue crystals were then obtained.

S3. The Figures in Supporting Information

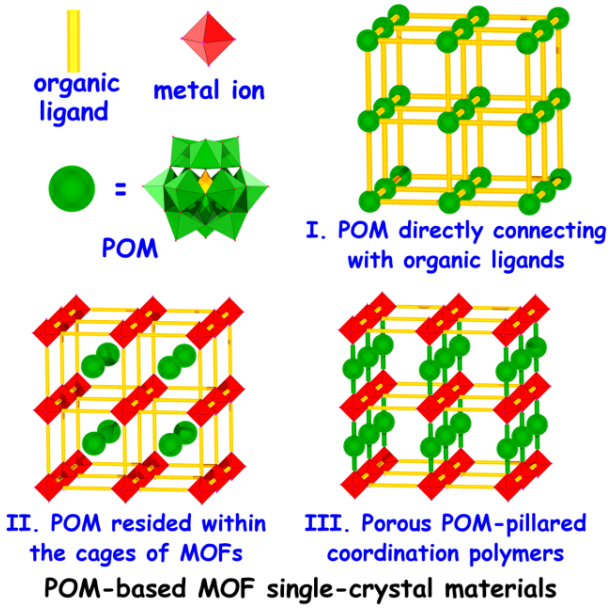

Figure S1. The three main forms associated with POM-based MOF materials.

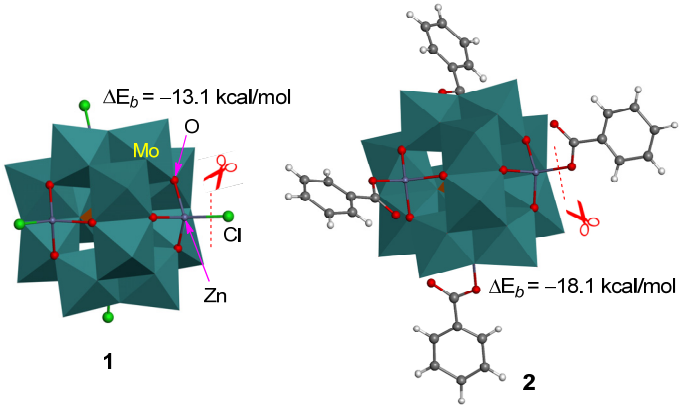

Figure S2. Decomposition definition for systems **1** and **2** and the calculated binding energies (ΔE_b) at the ground state.

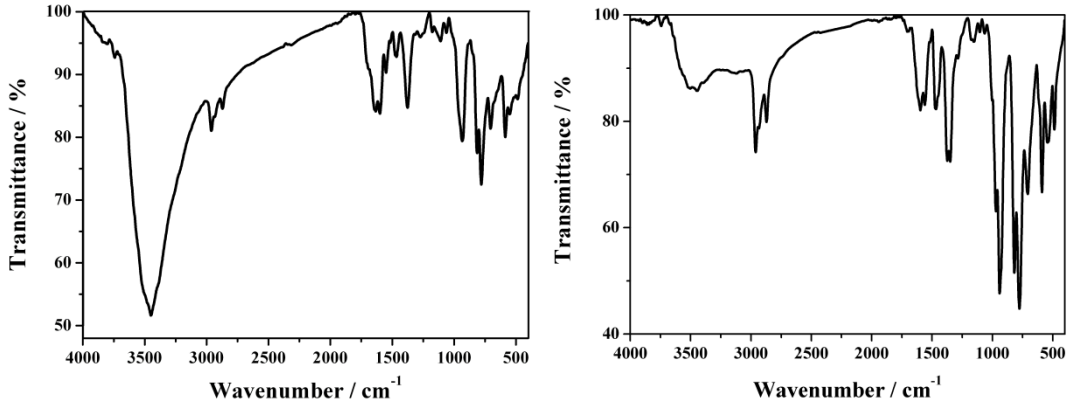

Figure S3. The IR curves of **NENU-500** (*left*) and **NENU-501** (*right*), respectively.

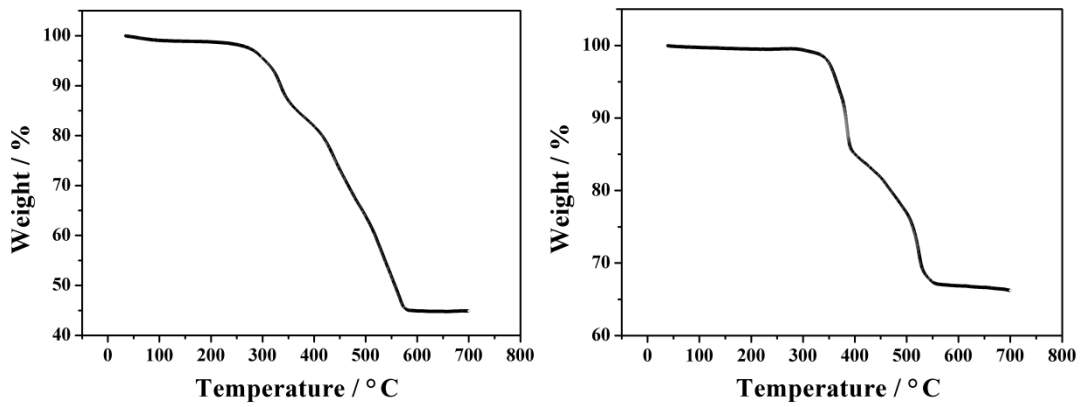

Figure S4. The TGA curves of **NENU-500** (*left*) and **NENU-501** (*right*) measured in air from room temperature to 700 °C at the heating rate of 5 °C·min^{-1}.

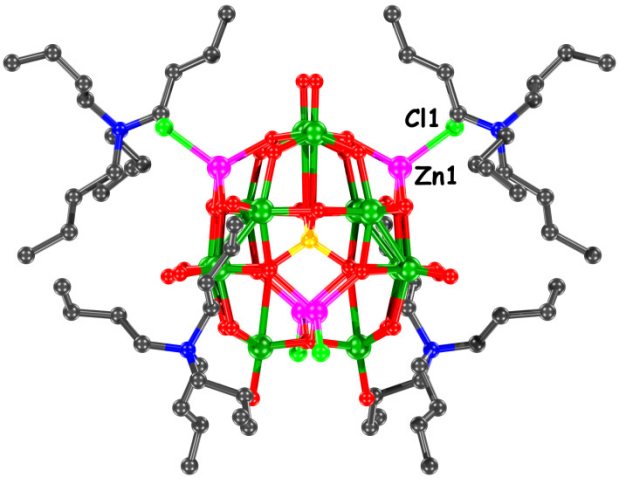

Figure S5. The asymmetric unit of **NENU-499**.

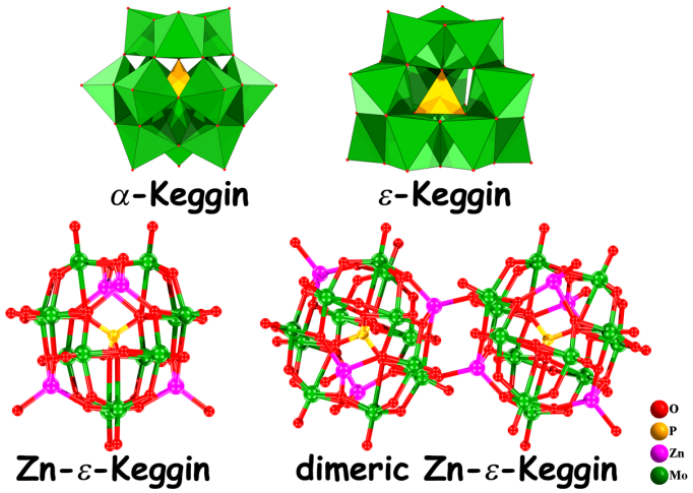

Figure S6. The comparisons of α-Keggin unit and ε-Keggin unit and the monomeric and dimeric forms of ε-Keggin.

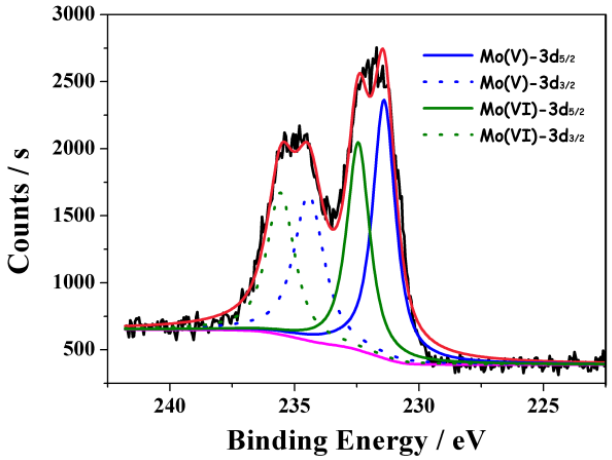

Figure S7. The XPS analysis of Mo element in **NENU-499**.

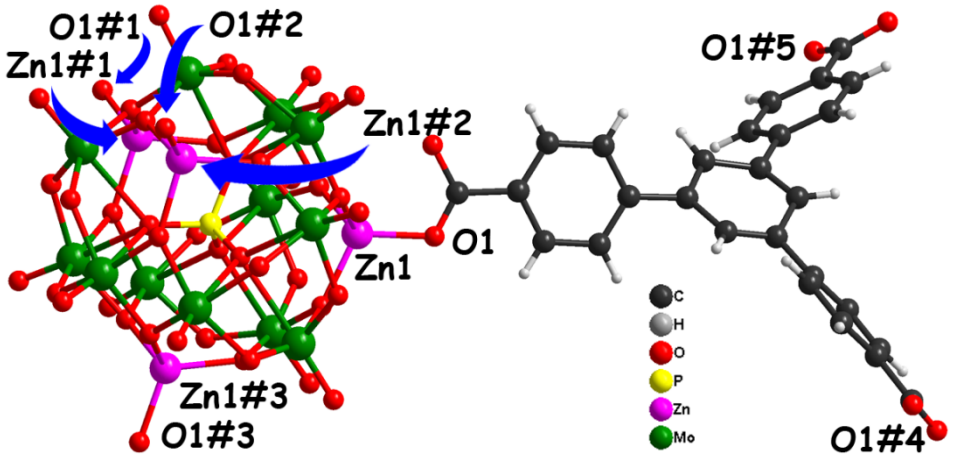

Figure S8. The coordination environments of Zn(II) centers in **NENU-500**. Symmetry codes: #1 0.75 – *x*, –0.25 + *z*, 0.25 – *y*; #2 0.75 – *x*, 0.25 – *z*, 0.25 + *y*; #3 *x*, –*y*, 0.5 – *z*; #4 0.5 + *z*, 0.5 – *x*, –*y*; #5 0.5 – *y*, – *z*, –0.5 + *x*.

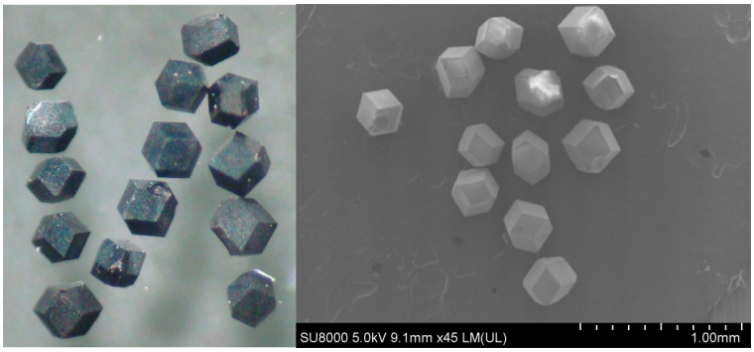

Figure S9. The images of **NENU-500** under optical microscope (*left*) and under scanning electron microscope (*right*), respectively.

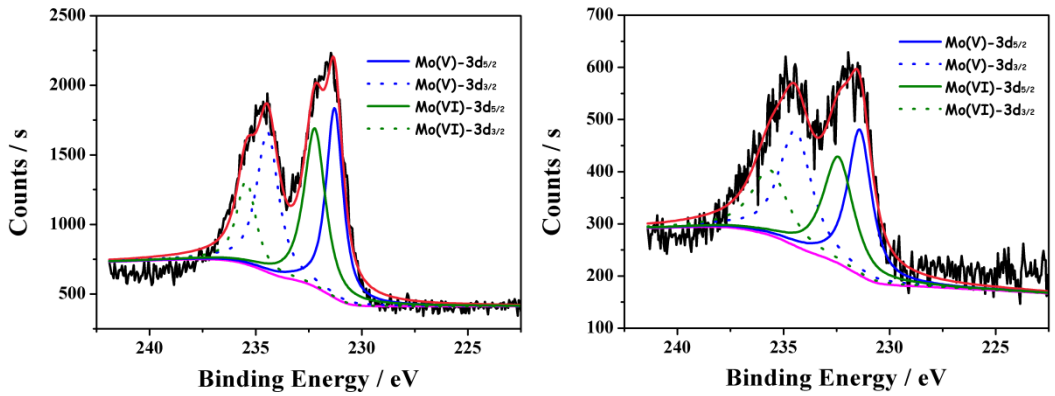

Figure S10. The XPS analysis of Mo element in **NENU-500** (*left*) and **NENU-501** (*right*), respectively.

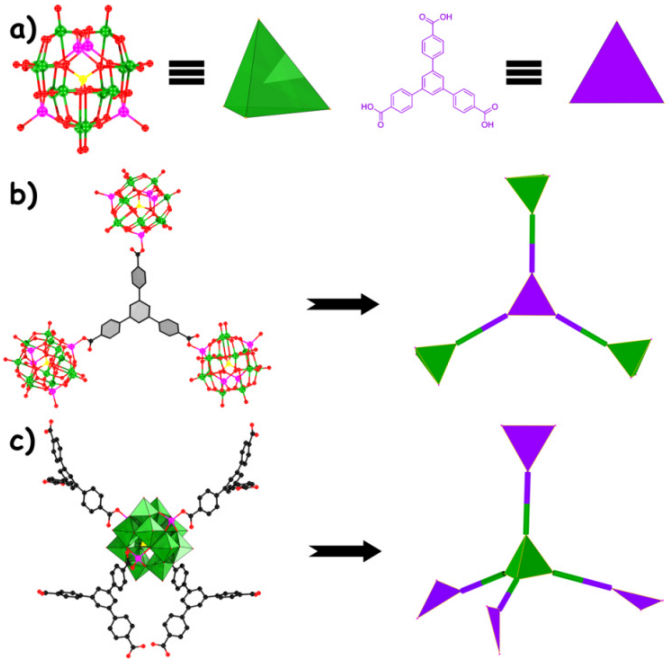

Figure S11. The 4-connected node of Zn-ε-Keggin unit and 3-connected linker of BPT^{3-} fragment in **NENU-500**, respectively.

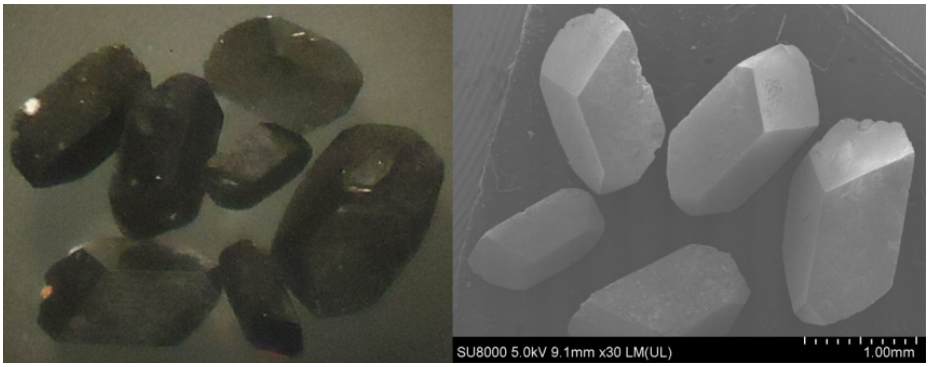

Figure S12. The images of **NENU-501** under optical microscope (*left*) and under scanning electron microscope (*right*), respectively.

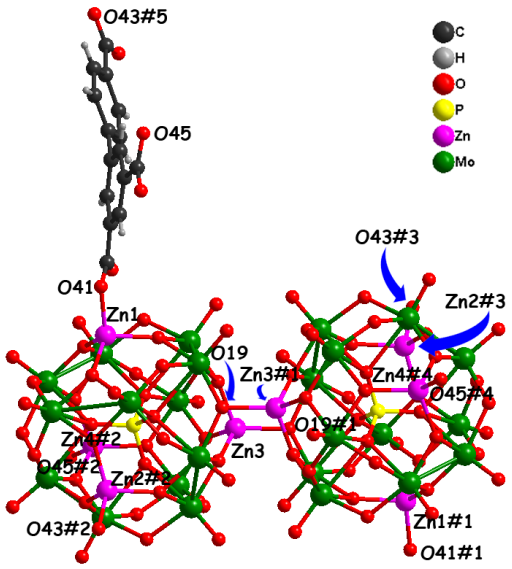

Figure S13. The coordination environments of Zn(II) centers in **NENU-501**. Symmetry codes: #1 1.5 – *x*, 2.5 – *y*, 1 – *z*; #2 *x*, 2 – *y*, –0.5 + *z*; #3 1.5 – *x*, 0.5 + *y*, 1.5 – *z*; #4 1.5 – *x*, 0.5 + *y*, 1.5 – *z*; #5 –0.5 + *x*, 1.5 – *y*, –0.5 + *z*.

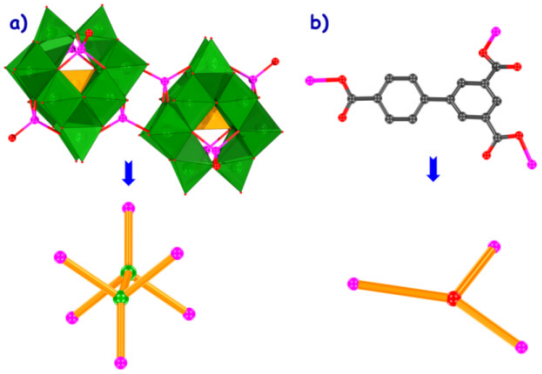

Figure S14. The connection modes of dimeric Zn-ε-Keggin unit and BPT^{3-} fragment in **NENU-501**, respectively.

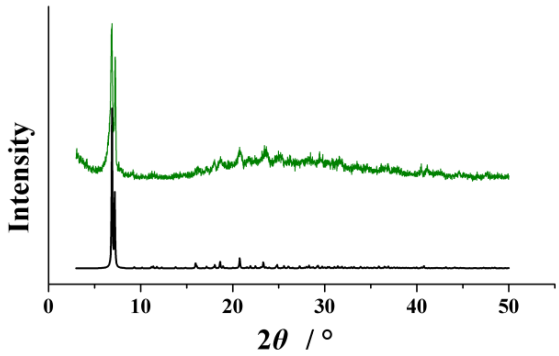

Figure S15. The PXRD patterns of **NENU-499**: simulated pattern (*black*) and as-synthesized sample (*green*), respectively.

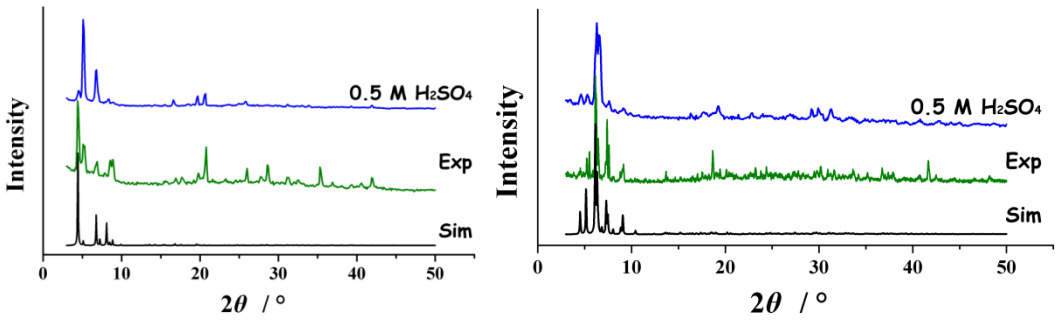

Figure S16. The PXRD patterns of **NENU-500** (*left*) and **NENU-501** (*right*): the simulated and experimental patterns and the as-synthesized samples in 0.5 M H_2SO_4 for 6 h, respectively.

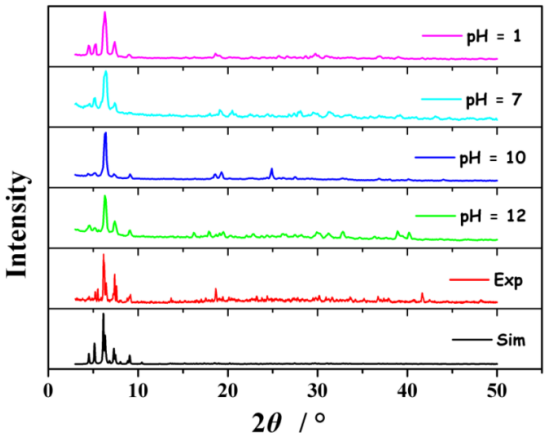

Figure S17. The PXRD patterns of **NENU-501** immersed in water at room temperature for 24 h at different pH. **Sim** represents the simulated pattern and **Exp** represents the pattern of as-synthesized sample, respectively.

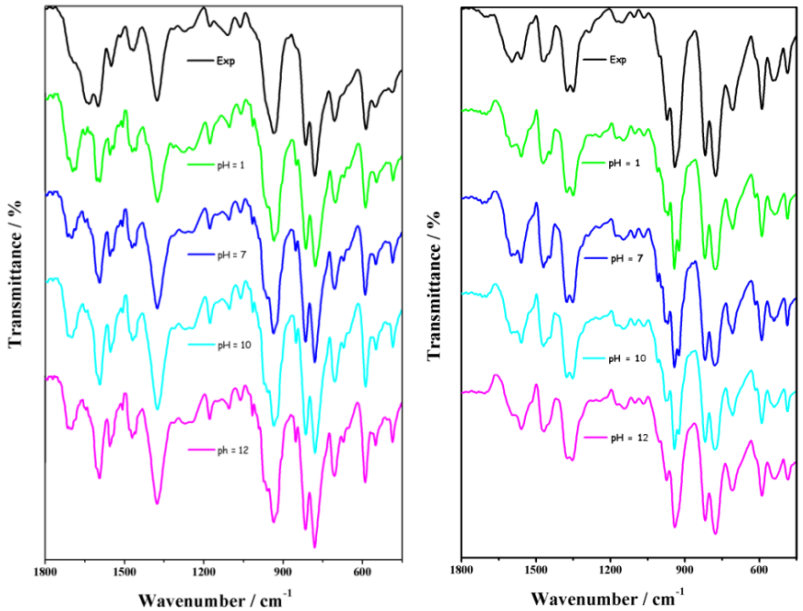

Figure S18. The IR curves of **NENU-500** (*left*) and **NENU-501** (*right*) immersed in water at different pH for 24 h, **Exp** represents the curve of the as-synthesized sample.

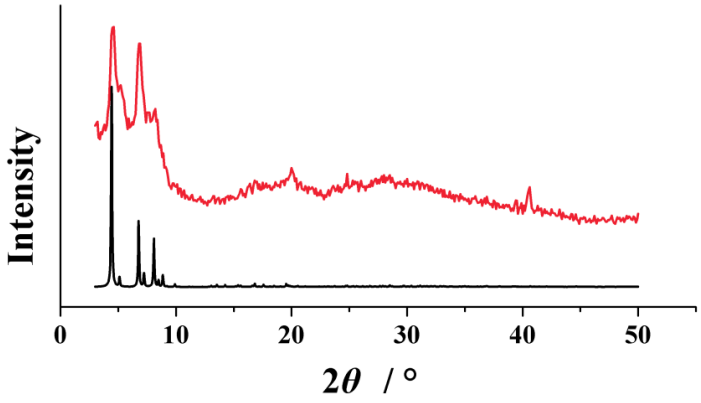

Figure S19. The PXRD patterns of **NENU-500**: simulated pattern (*black*) and after immersed in methanol for 3 days (*red*), respectively.

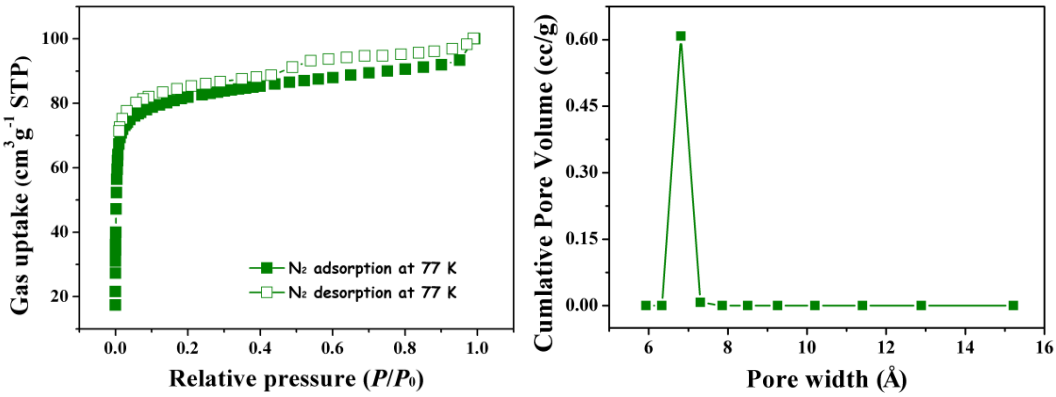

Figure S20. The nitrogen sorption isotherms of **NENU-500**a (*left*) recorded at 77 K and the pore size distribution of **NENU-500** (*right*), respectively.

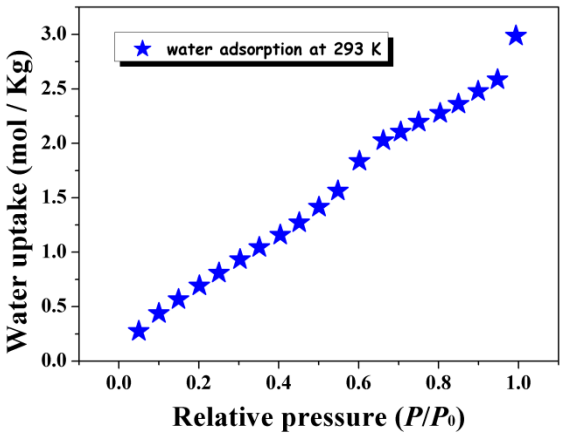

Figure S21. Water sorption isotherm for **NENU-500** measured at 293 K.

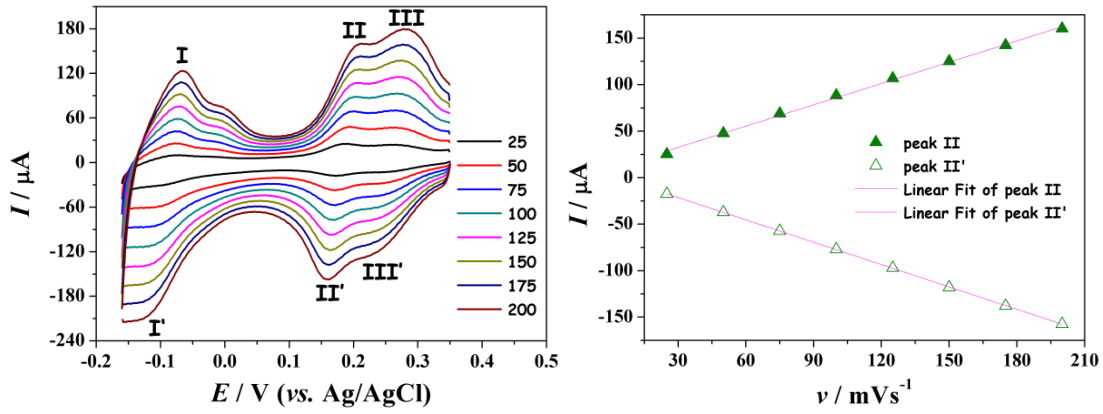

Figure S22. *Left*: The cyclic voltammograms of **NENU-499**-GCE measured in 0.1 mol·L^{-1} H_2SO_4 aqueous solution at different scan rates (mV·s^{-1}), respectively. *Right*: The plots and linear fits of the II-II' peak currents against scan rates for **NENU-499**–GCE, respectively.

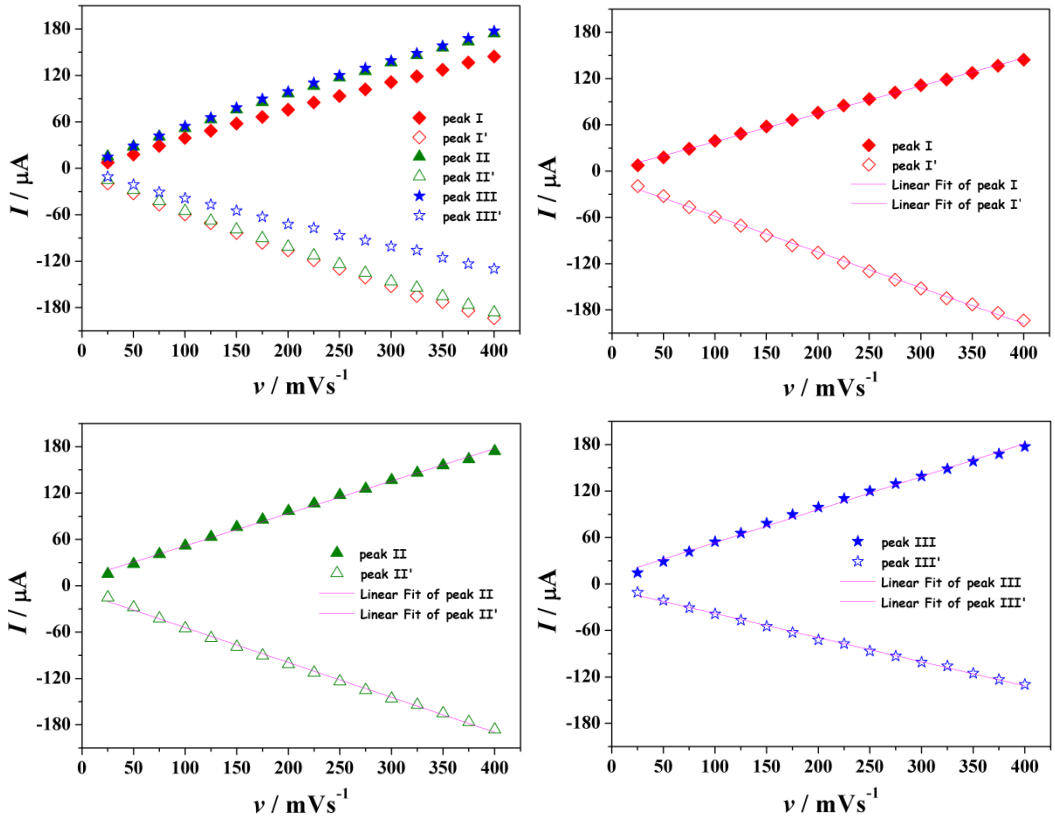

Figure S23. The plots and linear fits of the anodic and the cathodic peaks currents against scan rates for **NENU-500**–GCE, respectively.

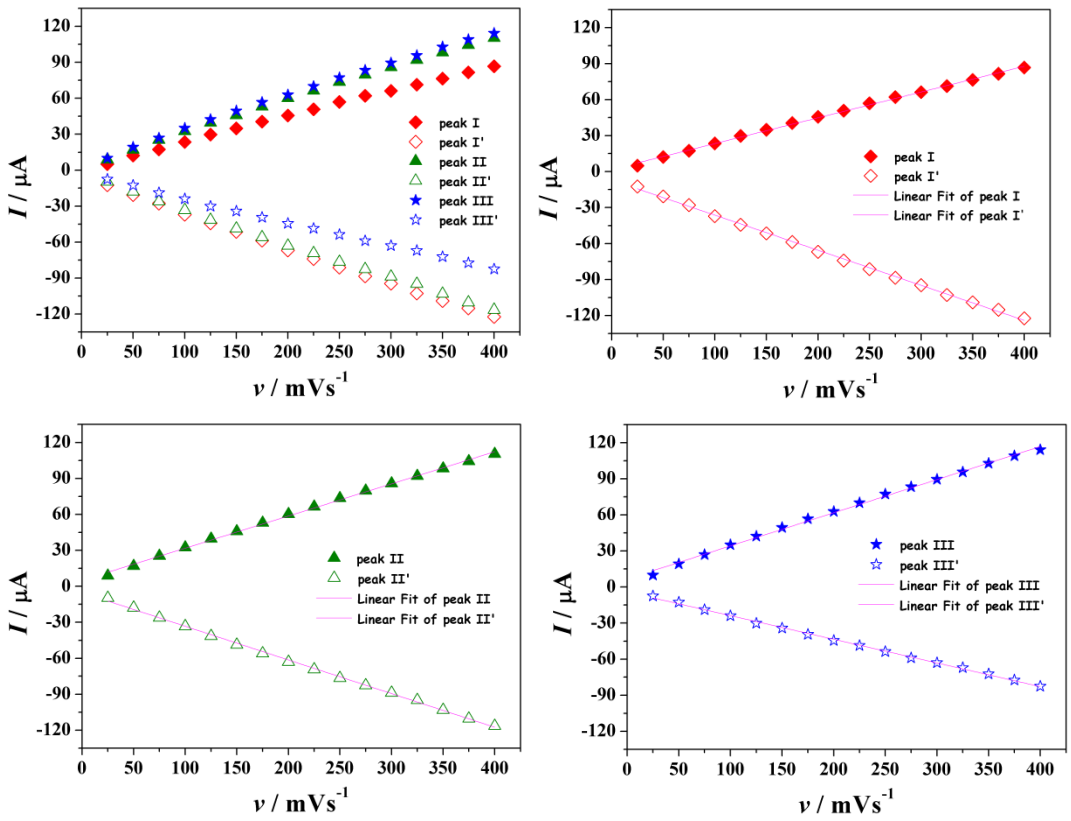

Figure S24. The plots and linear fits of the anodic and the cathodic peaks currents against scan rates for **NENU-501**–GCE, respectively.

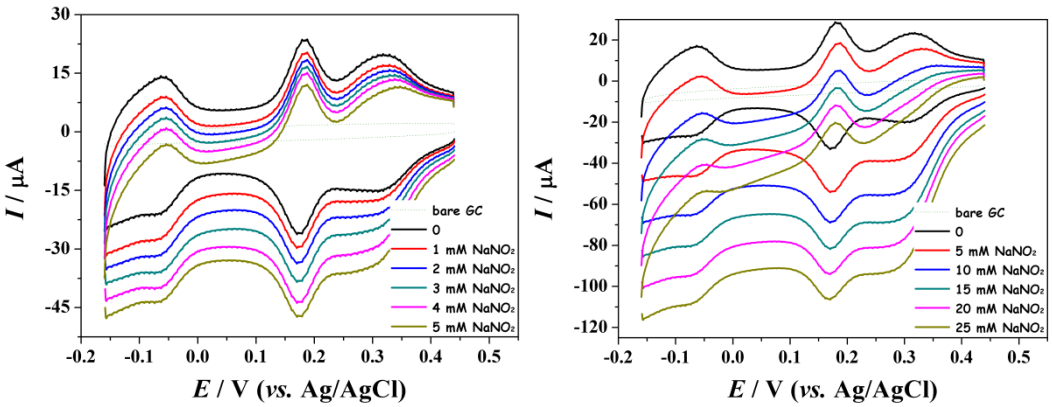

Figure S25. The cyclic voltammograms of **NENU-500**-GCE measured in 0.1 mol·L^{-1} H_2SO_4 aqueous solution containing different concentrations of $NaNO_2$ (at the scan rate of 50 mV·s^{-1}), respectively.

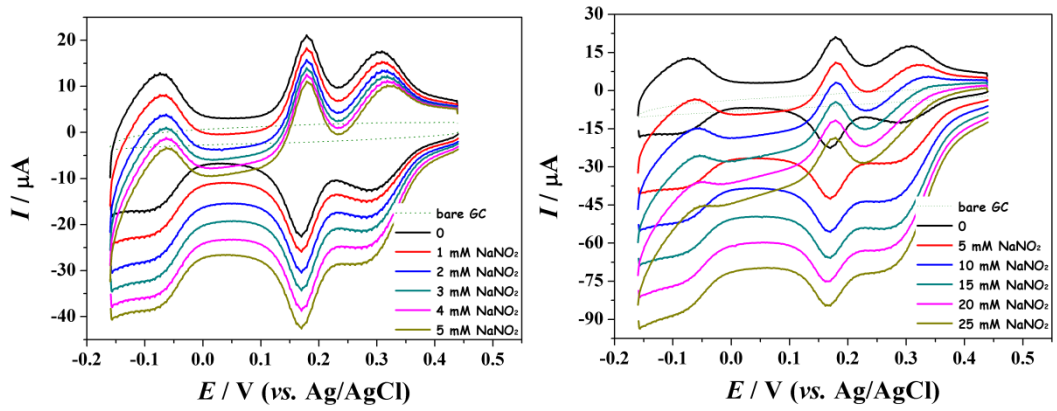

Figure S26. The cyclic voltammograms of **NENU-501**-GCE measured in 0.1 mol·L^{-1} H_2SO_4 aqueous solution containing different concentrations of $NaNO_2$ (at the scan rate of 50 mV·s^{-1}), respectively.

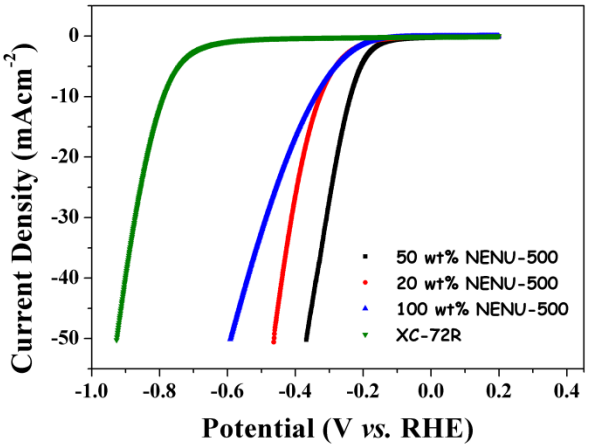

Figure S27. The polarization curves of **NENU-500** in 0.5 M H_2SO_4 aqueous solution at a scan rate of 5 mV·s^{-1}.

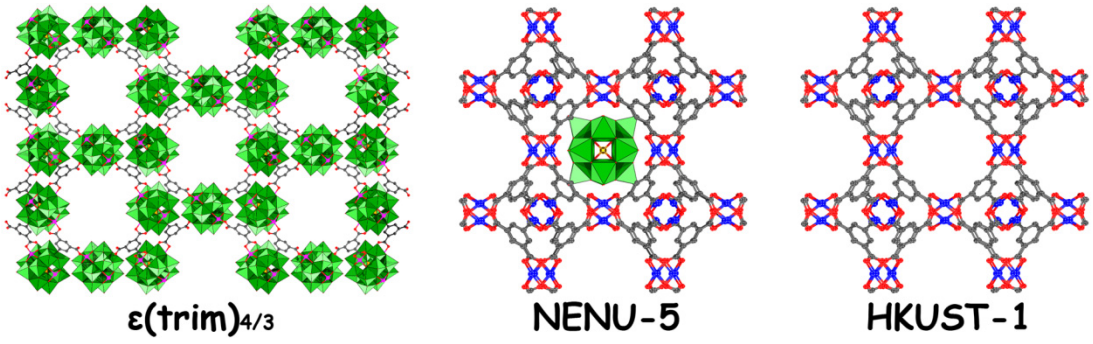

Figure S28. The structures of ***ε*(trim)$_{4/3}$**, **NENU-5** and **HKUST-1**.

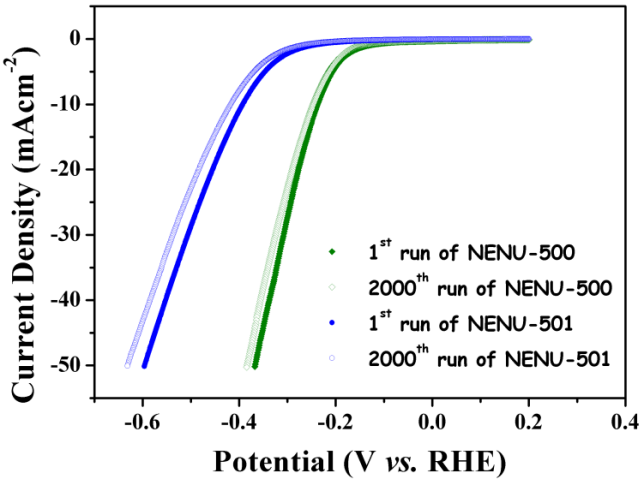

Figure S29. Polarization curves of **NENU-500** and **NENU-501** initially in 0.5 M H_2SO_4 aqueous solution and after 2000 cycles.

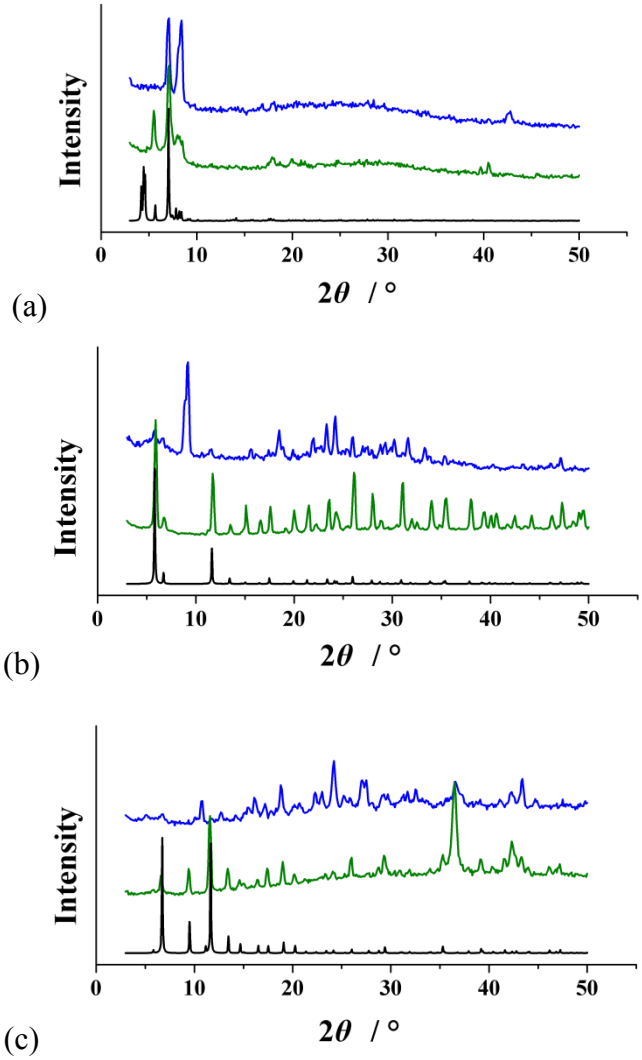

Figure S30. The PXRD patterns of (a) **ε(trim)$_{4/3}$**, (b) **NENU-5**, and (c) **HKUST-1**: the simulated pattern (*black*), the as-synthesized sample (*green*), and the as-synthesized samples in 0.5 M H_2SO_4 for 6 h (*blue*), respectively.

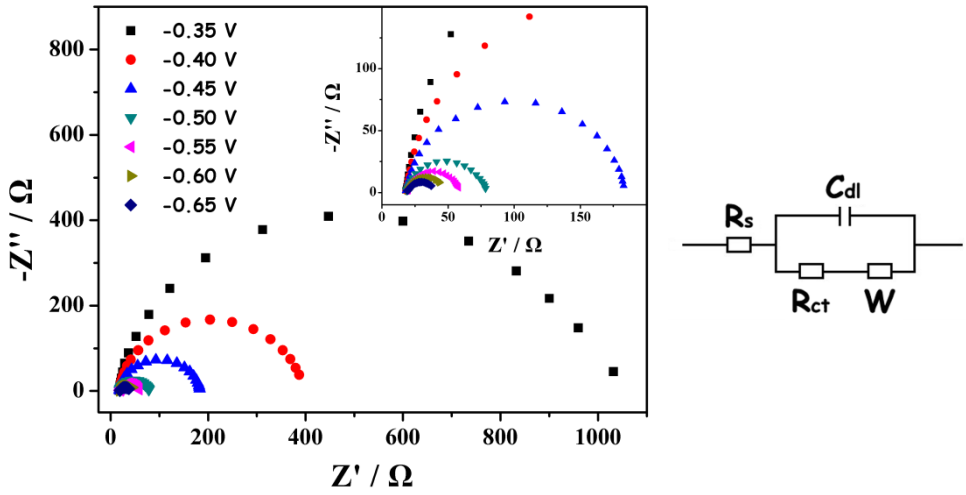

Figure S31. Nyquist plots of **NENU-501** examined at different potentials. Inset denotes the magnified image of high frequency region (*left*) and the equivalent circuit used for **NENU-500**/Vulcan carbon and **NENU-501**/Vulcan carbon (*right*). R_{ct}: the charge-transfer resistance at the surface of the catalysts, R_s: the solution resistance, C_{dl}: the capacitance, and W: Walburg impedance.

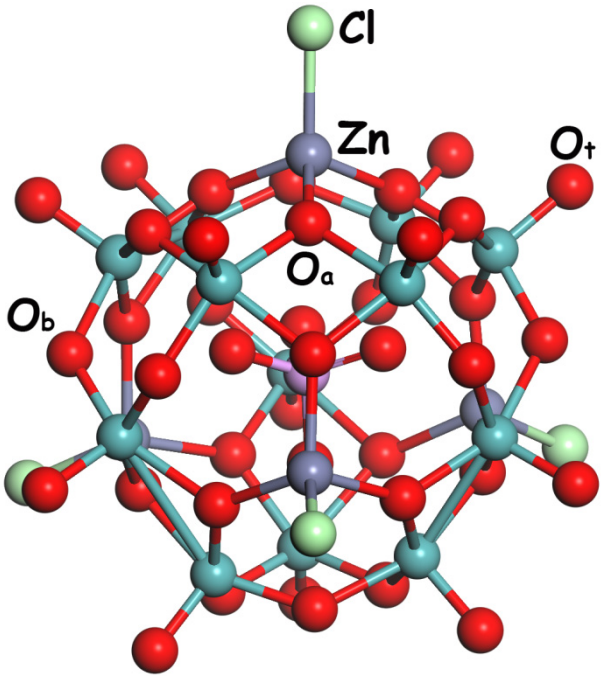

Figure S32. The calculated model for H adsorption sites on Zn-*ε*-Keggin-Cl unit.

S4. The Tables in Supporting Information

Table S1. Calculated relative energies (ΔE) at various spin multiplicities for systems **1** and **2**

system	**1**					**2**				
spin multiplicity	1	3	5	7	9	1	3	5	7	9
ΔE (kcal/mol)	0.0	27.2	60.5	97.4	132.4	0.0	0.1	17.9	37.3	61.1

Table S2. Crystal data and structure refinements for **NENU-499** – **NENU-501**

	NENU-499	**NENU-500**	**NENU-501**
Empirical formula	$C_{64}H_{147}Cl_4Mo_{12}N_4O_{40}PZn_4$	$C_{84}H_{132}Mo_{12}N_3O_{48}PZn_4$	$C_{63}H_{118}Mo_{12}N_3O_{46}PZn_4$
*M*w	3198.39	3395.97	3097.33
Crystal system	Tetragonal	Cubic	Monoclinic
Space group	*P*-42$_1$*c*	*Ia*-3*d*	*C*2/*c*
a (Å)	17.3920(12)	48.9280(13)	28.8818(13)
b (Å)	17.3920(12)	48.9280(13)	27.4017(13)
c (Å)	18.9820(12)	48.9280(12)	26.7889(12)
β (deg)	90	90	104.860
V (Å^3)	5741.7(7)	117131(5)	20491.9(16)
Z	2	24	8
D_c (Mg·m^{-3})	1.850	1.266	2.006
Abs.coeff. (mm^{-1})	2.256	1.293	2.428
R_{int}	0.0564	0.1434	0.0281
F(000)	3172	44640	12168
reflns collected	28396	291899	53295
Independent reflns	5077	8620	18105
GOF on F^2	1.030	1.004	1.040
R_1 [$I > 2\sigma(I)$][a]	0.0392	0.0693	0.0461
wR_2 [$I > 2\sigma(I)$][a]	0.0988	0.1664	0.1357
R_1 (all data)[b]	0.0552	0.2090	0.0650
wR_2 (all data)[b]	0.1079	0.2045	0.1509

[a] $R_1 = \Sigma||F_o| - |F_c||/\Sigma|F_o|$. [b] $wR_2 = |\Sigma w(|F_o|^2 - |F_c|^2)|/\Sigma|w(F_o^2)^2|^{1/2}$.

Table S3. The valence bond calculations for **NENU-499** – **NENU-501**

NENU-499		**NENU-500**		**NENU-501**	
P1	4.591	P1	4.820	P1	4.552
Zn1	1.983	Zn1	2.020	Zn1	1.983
				Zn2	2.040
				Zn3	1.961
				Zn4	2.072
Mo1	5.235	Mo1	5.252	Mo1	5.148
Mo2	5.099	Mo2	5.529	Mo2	5.064
Mo3	5.878	Mo3	5.499	Mo3	5.144
				Mo4	5.023
				Mo5	5.157
				Mo6	5.247
				Mo7	5.869
				Mo8	5.784
				Mo9	5.044
				Mo10	5.357
				Mo11	5.761
				Mo12	5.768

Table S4. The R_{ct} of **NENU-500** and **NENU-501** extracted from fitting electrochemical impedance spectra measured at different potential to an equivalent circuit

potential / mV (*vs.* Ag/AgCl)	R_{ct} for **NENU-500** / Ω	R_{ct} for **NENU-501** / Ω
–350	447	973
–400	170	374
–450	86	166
–500	45	61
–550	28	58
–600	16	39
–650	10	27

Reference

(1) (a) Becke, A. D. *Phys. Rev. A* **1988**, *38*, 3098–3100. (b) Becke, A. D. *J. Chem. Phys.* **1993**, *98*, 5648–5652. (c) Perdew, J. P.; Wang, Y. *Phys. Rev. B* **1992**, *45*, 13244–13249.

(2) Hay, P. J.; Wadt, W. R. *J. Chem. Phys.* **1985**, *82*, 270–283.

(3) (a) Barone, V.; Cossi, M. *J. Phys. Chem. A* **1998**, 102, 1995–2001. (b) Cossi, M.; Rega, N.; Scalmani, G.; Barone, V. *J. Comput. Chem.* **2003**, *24*, 669–681. (c) Tomasi, J.; Mennucci, B.; Cammi, R. *Chem. Rev.* **2005**, *105*, 2999–3093.

(4) Gaussian 09, Revision D.01, Frisch, M. J.; Trucks, G. W.; Schlegel, H. B.; Scuseria, G. E.; Robb, M. A.; Cheeseman, J. R.; Scalmani, G.; Barone, V.; Mennucci, B.; Petersson, G. A.; Nakatsuji, H.; Caricato, M.; Li, X.; Hratchian, H. P.; Izmaylov, A. F.; Bloino, J.; Zheng, G.; Sonnenberg, J. L.; Hada, M.; Ehara, M.; Toyota, K.; Fukuda, R.; Hasegawa, J.; Ishida, M.; Nakajima, T.; Honda, Y.; Kitao, O.; Nakai, H.; Vreven, T.; Montgomery, Jr., J. A.; Peralta, J. E.; Ogliaro, F.; Bearpark, M.; Heyd, J. J.; Brothers, E.; Kudin, K. N.; Staroverov, V. N.; Kobayashi, R.; Normand, J.; Raghavachari, K.; Rendell, A.; Burant, J. C.; Iyengar, S. S.; Tomasi, J.; Cossi, M.; Rega, N.; Millam, J. M.; Klene, M.; Knox, J. E.; Cross, J. B.; Bakken, V.; Adamo, C.; Jaramillo, J.; Gomperts, R.; Stratmann, R. E.; Yazyev, O.; Austin, A. J.; Cammi, R.; Pomelli, C.; Ochterski, J. W.; Martin, R. L.; Morokuma, K.; Zakrzewski, V. G.; Voth, G. A.; Salvador, P.; Dannenberg, J. J.; Dapprich, S.; Daniels, A. D.; Farkas, Ö.; Foresman, J. B.; Ortiz, J. V.; Cioslowski, J.; Fox, D. J. Gaussian, Inc., Wallingford CT, **2009**.

(5) Delley, B. *J. Chem. Phys.* **2000**, *113*, 7756–7764.

(6) Perdew, J. P.; Burke, K.; Ernzerhof, M. *Phys. Rev. Lett.* **1996**, *77*, 3865–3868.

(7) Nohra, B.; Moll, H. E.; Albelo, L. M. R.; Mialane, P.; Marrot, J.; Mellot-Draznieks, C.; O'Keeffe, M.; Biboum, R. N.; Lemaire, J.; Keita, B.; Nadjo, L.; Dolbecq, A. *J. Am. Chem. Soc.* **2011**, *133*, 13363–13374.

(8) Sun, C.-Y.; Liu, S.-X.; Liang, D.-D.; Shao, K.-Z.; Ren, Y.-H.; Su, Z.-M. *J. Am. Chem. Soc.* **2009**, *131*, 1883–1888.

(9) Chui, S. S.-Y.; Lo, S. M.-F.; Charmant, J. P. H.; Orpen, A. G.; Williams, I. D. *Science* **1999**, *283*, 1148–1150.